Environmental Science & Technology

Article

pubs.acs.org/est

Effective Henry's Law Partitioning and the Salting Constant of Glyoxal in Aerosols Containing Sulfate

Christopher J. Kampf,[†] Eleanor M. Waxman,[†,‡] Jay G. Slowik,[§] Josef Dommen,[§] Lisa Pfaffenberger,[§] Arnaud P. Praplan,[§] André S. H. Prévôt,[§] Urs Baltensperger,[§] Thorsten Hoffmann,[∥] and Rainer Volkamer*[,†,‡]

[†]Department of Chemistry and Biochemistry, University of Colorado, UCB 215, Boulder, Colorado, United States

[‡]CIRES, University of Colorado, UCB 216, Boulder, Colorado, United States

[§]Laboratory of Atmospheric Chemistry, Paul Scherrer Institut, Villigen, Switzerland

[∥]Institute for Inorganic and Analytical Chemistry, Johannes Gutenberg-University, Mainz, Germany

Supporting Information

ABSTRACT: The reversible partitioning of glyoxal was studied in simulation chamber experiments for the first time by time-resolved measurements of gas-phase and particle-phase concentrations in sulfate-containing aerosols. Two complementary methods for the measurement of glyoxal particle-phase concentrations are compared: (1) an offline method utilizing filter sampling of chamber aerosols followed by HPLC-MS/MS analysis and (2) positive matrix factorization (PMF) analysis of aerosol mass spectrometer (AMS) data. Ammonium sulfate (AS) and internally mixed ammonium sulfate/fulvic acid (AS/FA) seed aerosols both show an exponential increase of effective Henry's law coefficients ($K_{H,eff}$) with AS concentration (c_{AS}, in mol kg^{-1} aerosol liquid water, m = molality) and sulfate ionic strength, $I(SO_4^{2-})$ (m). A modified Setschenow plot confirmed that "salting-in" of glyoxal is responsible for the increased partitioning. The salting constant for glyoxal in AS is $K^S_{CHOCHO} = (-0.24 \pm 0.02)\ m^{-1}$, and found to be independent of the presence of FA. The reversible glyoxal uptake can be described by two distinct reservoirs for monomers and higher molecular weight species filling up at characteristic time constants. These time constants are $\tau_1 \approx 10^2$ s and $\tau_2 \approx 10^4$ s at $c_{AS} < 12\ m$, and about 1−2 orders of magnitude slower at higher c_{AS}, suggesting that glyoxal uptake is kinetically limited at high salt concentrations.

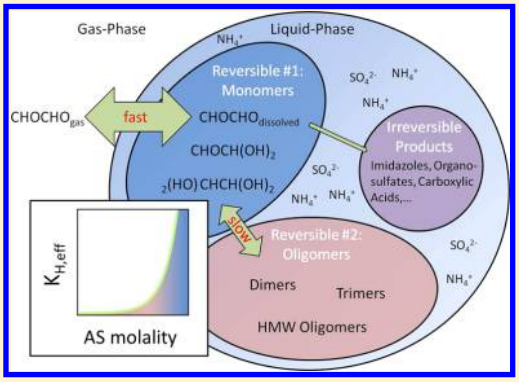

1. INTRODUCTION

Secondary organic aerosols (SOA) are attracting increasing attention in atmospheric research owing to their impacts on climate forcing, air quality, visibility, and public health. Improving knowledge about formation and transformation processes of SOA is necessary to reduce the uncertainties related to the radiative forcing of aerosols,[1] as SOA makes up about 30−60% of ambient organic aerosols (OA) in urban environments, and even higher fractions (>70%) in rural areas.[2−4] Recent modeling studies report SOA formation from the volatile α-dicarbonyl compounds glyoxal (Gly) and methylglyoxal (Mgly) to be on the order of 5−11 Tg a^{-1} on a global scale, thus being of a magnitude comparable to the sum of SOA formed from other oxidation products of mono- and sesquiterpenes, isoprene, and aromatics.[5,6]

Reversible and irreversible condensed-phase reactions of these compounds yield products of lower volatility; e.g. acetal and aldol oligomer formation[7−12] and NH_4^+ incorporation products (imines, imidazoles).[15−25] Also organo-sulfate formation[9,13,14] and the irreversible oxidation by OH radicals yielding carboxylic acids (e.g. oxalic acid or pyruvic acid) have been observed.[26−30]

Glyoxal uptake into a dilute aqueous phase in the atmosphere (e.g. fog or cloudwater) follows the Henry's law equilibrium observed for bulk aqueous phases, e.g. for pure water:[31]

$$[\mathrm{Gly}]_p = K_H \times [\mathrm{Gly}]_g \quad (1)$$

where $[\mathrm{Gly}]_g$ (atm) and $[\mathrm{Gly}]_p$ (mol L^{-1}) represent the concentrations of glyoxal in the gas-phase and particle-phase, respectively, and K_H (mol L^{-1} atm^{-1}) is the Henry's law coefficient. Experimentally determined K_H values for glyoxal are always affected by hydration of the carbonyl functional groups. These effective Henry's law coefficients ($K_{H,eff}$) can be expressed as

$$K_{H,eff} = K_H \times (1 + K_{hyd1} + K_{hyd1} \times K_{hyd2}) \quad (2)$$

Received: January 6, 2013
Revised: March 24, 2013
Accepted: March 27, 2013
Published: March 27, 2013

   dx.doi.org/10.1021/es400083d | Environ. Sci. Technol. 2013, 47, 4236−4244

Table 1. Overview of the Experiments Conducted for This Work

	RH (%)[a]	$[Gly]_g$ (ppbv)[b]		d_{seed} (nm)[d]	FA:SO_4^{2-} [e]	CONT:SO_4^{2-} [f]	$K_{H,eff}$ (10^7 m atm^{-1})[g]	
exp no.	mean ±1σ	mean ±1σ	m_{seed} ($\mu g\ m^{-3}$)[c]	mode	mean	mean	min	max
AS seed								
4	70 ± 3	9.8 ± 6.1	14	75	3%	6%	3.3	21.0
6	66 ± 1	12.6 ± 7.1	14	65	1%	7%	4.5	24.1
7	51 ± 1	15.8 ± 5.2	13	65	1%	5%	9.3	9.4
8	57 ± 1	8.5 ± 2.5	20	68	0%	4%	3.5	11.4
11	74 ± 3	10.1 ± 7.0	25	75	1%	3%	0.4	8.5
AS/FA seed								
3	68 ± 5	9.8 ± 6.3	20	115	5%	9%	2.0	29.7
5	52 ± 6	12.7 ± 4.3	60	91	242%	8%	3.8	32.8
9	57 ± 1	17.1 ± 4.3	31	150	118%	8%	5.8	8.4
10	57 ± 1	18.9 ± 5.7	25	80	119%	7%	5.7	15.4
12	74 ± 3	13.9 ± 9.2	37	75	112%	3%	0.7	5.8

[a]Averaged over the time period between 1st glyoxal addition and dilution of the chamber. [b]Glyoxal mixing ratio (CE-DOAS). [c]Dry seed mass at beginning of experiment. [d]Dry mode diameter of seed aerosol (AMS PToF). [e]Ratio of FA PMF factor to sulfate. [f]Ratio of contamination PMF factor (CONT) to sulfate (indicator for chamber background and/or seed contamination). [g]Effective Henry's law coefficient (calculated using results of offline glyoxal particle-phase analysis, see Supporting Information for details).

with the dimensionless equilibrium constants K_{hyd1} and K_{hyd2} representing the ratios of the rate constants for forward and backward reactions of the first and second hydration.[32]

The gas-/particle-phase equilibrium coefficients measured for aerosols are 2−3 orders of magnitude larger than for dilute aqueous phases.[33−36] Kroll et al.[33] proposed that the high salt concentration present in chamber seed aerosols (6.5−7.5 mol L^{-1}, M) was responsible for enhanced uptake due to a "salting-in" effect, while Ip et al.[31] showed that in bulk solutions ionic strength (or salt concentration) alone does not sufficiently describe the shifting in the gas-/particle-phase equilibrium of glyoxal toward the condensed phase. They proposed a "sulfate effect" due to a major enhancement of $K_{H,eff}$ already occurring at low sulfate ionic strengths, $I(SO_4^{2-})$, i.e. by a factor of ∼50 at $I(SO_4^{2-}) = 0.03$ M, while other ionic species, e.g. chloride ions, did not enhance $K_{H,eff}$ in a comparable manner.[31,33] The effect of inorganic ionic species on the solubility of organic compounds in aqueous solutions is known from early work by Setschenow in the late 19th century to cause exponentially increasing partitioning behavior with increasing salt concentration.[37] While for nonpolar or weakly polar organic compounds the solubility generally is decreased ("salting-out"), a "salting-in" effect can be observed for very polar compounds.[38] The magnitude of the salting effect depends on the organic compound as well as on the type of inorganic ions present in solution.

Previous chamber studies determined effective Henry's law coefficients for glyoxal based on the volume change of seed aerosols after glyoxal uptake.[33−36] While these previous studies focused on particle growth, product identification, and photochemical vs dark uptake processes, we present the first systematic study of the salting effect on glyoxal partitioning. Additionally, the temporal partitioning behavior of glyoxal was investigated. Further, results of an offline filter sampling method for the quantification of particulate glyoxal concentrations are compared to PMF analysis results of AMS data, which were used for the first time to calculate time-resolved $K_{H,eff}$ data.

2. EXPERIMENTAL SECTION

2.1. Smog Chamber Description. Experiments were conducted in the PSI smog chamber.[39] Briefly, the chamber consists of a 27 m^3 Teflon bag suspended in a temperature-controlled wooden housing. Two different light sources were used in this study: UV lights (Philips, Cleo performance 100W/R) for the photochemical production of glyoxal from the OH oxidation of acetylene, and visible lights (4 kW xenon arc lamps utilizing 410 nm long-pass filters to eliminate the UV component of the xenon arc lamps).

2.2. Materials. Eighteen MΩ cm water (Milli-Q water system, MilliPore, Bedford, MA) was passed through a heated pyrex bulb to humidify the chamber. $(NH_4)_2SO_4$ (AS) or $(NH_4)_2SO_4$/fulvic acid (AS/FA) solutions (FA = Suwannee River Fulvic Acid, sample 1R101F from the International Humic Substances Society, http://www.ihss.gatech.edu) were used to generate internally mixed seed particles with a nebulizer built in-house. From Experiment 6 onward, the AS solution concentration was 0.4 g L^{-1} (except for Experiments 7 and 8, which used 0.46 and 0.54 g L^{-1}, respectively) and the AS/FA solution was 0.4 g L^{-1} AS and 0.08 g L^{-1} FA. Concentrations in the earlier experiments were variable as the seed system was optimized. The seed particles were directly injected into the chamber (without drying). A sufficiently high RH was maintained inside the chamber to prevent particle efflorescence. From Experiment 5 onward, a diffusion tube filled with activated charcoal was installed between the nebulizer and the chamber to prevent volatile organic contaminants from entering the chamber with the seed. The charcoal was replenished after each experiment by baking at 500 °C for ∼24 h. HONO (approximately 10 ppbv at the start of each experiment) was used as a source of OH radicals and injected prior to each experiment. HONO was produced by reaction of $NaNO_2$ (0.003 M) and H_2SO_4 (0.01 M), which were continuously supplied to a reaction vessel using a peristaltic pump. The produced HONO was entrained into the chamber in a 2.5 slpm (standard liters per minute) flow of pure air.[40] Glyoxal was generated inside the chamber from the reaction of acetylene with OH radicals. Acetylene (99.7%) was passed through a liquid N_2/acetone slush bath to remove low-volatility impurities (mostly sulfur-containing compounds) before being injected into the chamber. Injections were performed at ∼0.5 slpm and lasted less than 1 min to attain ∼10 ppm acetylene in the chamber. NO (100 ppb) was injected into the chamber

from Experiment 5 onward to suppress formation of photochemically produced ozone (O_3) during UV light exposures.

2.3. Experimental Conditions. A typical experiment was conducted as follows. First, the chamber was humidified, then the seed aerosol and HONO were injected in sequence. The chamber was sealed and allowed to stand for 30 min to allow component mixing. Then a "blank" UV exposure was performed to generate OH radicals and determine the extent of SOA formation from residual organic chamber contaminants using the AMS. The UV light exposure was of the following form: 4 min UV on, 30 min off, 2 min UV on, and 30 min off to allow sufficient time for any contaminant SOA to form. Following the blank exposures, acetylene was added to the chamber, and 30 min was allowed for component mixing. Then the first experimental UV exposure was performed, with the following form: 3 min UV on, 3 min off, 3 min UV on. Glyoxal was formed in the presence of O_2 and NO from the following reactions:[41]

$$\mathrm{HONO} + h\nu \rightarrow \mathrm{OH} + \mathrm{NO} \quad \text{(R1)}$$

$$\mathrm{C_2H_2} + \mathrm{OH} \rightarrow \mathrm{C_2H_2O_2} + \mathrm{OH}\ (\sim 65\%\text{yield}) \quad \text{(R2)}$$

$$\mathrm{C_2H_2} + \mathrm{OH} \rightarrow \text{formaldehyde} + \mathrm{CO}\ (\sim 35\%\text{yield}) \quad \text{(R3)}$$

The chamber was left to stand for 3−4 h to allow glyoxal uptake and particle-phase reactions to proceed, then a second experimental UV exposure was performed, followed by another undisturbed 3−4 h. Additionally, some experiments included periods with the UV-filtered xenon lamps turned on (i.e. in the presence of visible light). At the end of each experiment, a dilution phase was initiated, where the chamber was diluted with pure air humidified to the same RH at which the experiment was run. An overview of the experimental conditions is given in Table 1.

2.4. Gas-Phase Measurements. The University of Colorado Light-Emitting-Diode Cavity-Enhanced Differential Optical Absorption Spectroscopy (CU LED-CE-DOAS) technique is described in detail in Thalman and Volkamer.[42] Briefly, light from a blue LED is focused into a 0.91 m long optical cavity consisting of a pair of highly reflective mirrors (reflectivity, R = 0.999962). The light exiting the cavity is coupled to a QE-65000 spectrometer (380−490 nm range) using a fiber optic cable. The sample flow (0.15 slpm) was combined with a dilution flow (0.45 slpm) outside of the chamber to reduce the relative humidity in the lines and minimize glyoxal losses to tubing walls. Immediately following this dilution a 2 μm Teflon filter was positioned to prevent aerosols from entering the cavity to minimize losses by Mie scattering. The instrument measured gas-phase glyoxal, NO_2, and oxygen dimers (O_4) from the chamber with a time resolution of 1 min, and a 30 pptv (chamber equivalent concentration) glyoxal detection limit, using WinDOAS software for spectral fitting, and is calibrated from absorption cross-section reference spectra for glyoxal,[43] NO_2,[44] O_4,[45] and water.[46]

NO_x, NO, and NO_2 were monitored by a 42C NO−NO_2−NO_x Analyzer (Thermo Environmental Instruments Inc., Waltham, MA, USA). NO_x was also measured by a ML 9841A NO_x Chemiluminescence Analyzer (Monitor Laboratories Inc., Englewood, CO, USA). O_3 was monitored with an Ozone Analyzer model 8810 (Monitor Laboratories Inc.) and a Series 300 Ozone Analyzer (Environics Inc., Tolland, CT, USA).

2.5. Particle-Phase Measurements. Two complementary techniques were applied to quantify the particulate glyoxal concentrations. One is based on traditional filter sampling, followed by highly specific HPLC-ESI-MS/MS detection. The other technique is based on the time-resolved online measurements of the aerosol chemical composition using an HR-ToF-AMS.

Filter samples for offline HPLC-ESI-MS/MS analysis were taken at selected times during each experiment. One to three filter samples collected prior to glyoxal production in the chamber served as individual blanks for each smog chamber experiment. Sampling times were 15−30 min at a flow rate of 4.49 L min^{-1}, depending on seed composition. Filters were stored in glass vessels with Teflon lined caps at −20 °C until analysis. Sample preparation and measurement conditions are described in Kampf et al.[47] Briefly, one half of each filter sample was extracted by sonication using 1:1 methanol/water (v/v) as the extracting reagent. Extracts were evaporated to 0.2 mL under a gentle N_2-stream at 45 °C. Bis-hydrazone derivatives of glyoxal were obtained by adding a 0.1 M solution of 2,4-dinitrophenylhydrazine in 40% sulfuric acid. Using this technique, glyoxal as well as its hydrated forms and reversibly formed oligomers are efficiently transformed into glyoxal-bis-2,4-dinitrophenylhydrazone, which was quantified by means of HPLC-ESI-MS/MS.

Size distributions were measured with a scanning mobility particle sizer (SMPS) built in-house, employing a CPC 3022 (TSI, Inc., Shoreview, MN, USA). SMPS data are limited to experiments 3−8. Particle number concentrations were measured with a TSI CPC 3025. The SMPS operates with a recirculating, filtered air system. The relative humidity inside the SMPS is therefore assumed to be the same as in the chamber and no significant mass loss due to water evaporation is expected.

Online measurements of particle composition were performed by a high-resolution time-of-flight aerosol mass spectrometer (HR-ToF-AMS, Aerodyne Research, Inc., Billerica, MA, USA). The working principles of the HR-ToF-AMS have been described in the literature.[48] Analysis of mass spectral fragmentation patterns yields quantitative concentrations of species such as organics or sulfate.[49] The HR-ToF-AMS also has sufficient resolving power to quantitatively resolve individual ions at the same nominal m/z.[50] A detailed discussion on the bounce collection efficiency of the AMS (E_b), i.e. probability for detection of impacting particles, can be found in the Supporting Information. For this study E_b = 0.54 was used for the entire set of experiments.

2.6. Data Analysis Methods. Aerosol liquid water content (ALWC, kg m^{-3}) was calculated using the aerosol inorganics model (AIM-IV), a temperature-dependent thermodynamics model.[51,52] Input ammonium, sulfate, and organics concentrations were taken from the AMS data. Chloride and nitrate were present in quantities at least an order of magnitude less than sulfate and were neglected in calculations. Analysis conditions assumed deliquesced aerosols. The AMS organic time trace was used as a proxy for FA in AIM-IV, assuming a molecular weight (MW) of 150 g mol^{-1} (see Supporting Information and Table S3) and a molar volume[53] of 4.39 cm^3 mol^{-1} at pH 4.

HR-ToF-AMS organic mass spectra (high-resolution for m/z 12 to 115; unit mass resolution for m/z 116 to 300) were analyzed using positive matrix factorization (PMF),[54,55] which represents the mass spectral time series as a linear combination

of static factors (i.e. mass spectra) and their time-dependent intensities. Protocols for PMF analysis of AMS data have been discussed in detail in the literature.[56,57] Four meaningful factors were resolved: (1) fulvic acid seed ("FA"); (2) glyoxal + reversibly forming compounds ("GLY"); (3) glyoxal SOA ("SOA"); and (4) organic contaminants entering the chamber with the AS seed ("CONT"). The "GLY" factor, containing glyoxal, its hydrates, and presumably its oligomers, were used for AMS-based $K_{H,eff}$ calculations. The parametrizations derived from the GLY factor represent lower limits for predicting glyoxal SOA mass. Detailed information on the PMF analysis is given in the Supporting Information.

3. RESULTS AND DISCUSSION

3.1. Effect of Ammonium Sulfate Concentration in Seed Aerosols on $K_{H,eff}$. Monitoring aerosol chemical composition with the AMS allowed for time-resolved calculations of ALWC during the experiments conducted for this work. Therefore, aqueous phase AS concentrations, c_{AS} = AS_{AMS}/ALWC (mol kg^{-1}, m), with AS_{AMS} = AMS ammonium sulfate concentration (mol m^{-3}), in the particles could be calculated and averaged for the respective times of the filter sampling periods to investigate the effect on glyoxal partitioning. The analysis of correlations between $K_{H,eff}$ (offline HPLC-MS/MS) and c_{AS} showed an exponential increase of $K_{H,eff}$ with c_{AS}. In a modified Setschenow plot[37] $\log(K_{H,w}/K_{H,salt})$, with $K_{H,w}$ = effective Henry's law coefficient in pure water and $K_{H,salt}$ = effective Henry's law coefficient in AS containing seed particles, is plotted versus c_{AS}. The slope of the resulting linear regression gives the salting constant for glyoxal, K^S_{CHOCHO}, as shown in Figure 1. Although in the original definition by Setschenow the $\log(K_{H,w}/K_{H,salt})$ is plotted vs the total salt concentration, c_{Salt} (mol L^{-1}), we use molality of glyoxal and AS in aerosol liquid water for both K_H and c_{AS}, because in this notation the presence of organic material in the seed particles (FA) did not have a significant influence (see below). However, when using the total seed volume for partitioning, or molarity of the salt concentration, a seed influence is visible (see Figure S1 in the Supporting Information). No effect of visible light on the reversible partitioning of glyoxal was observed. The data shown cover all samples, from periods with and without visible lights turned on.

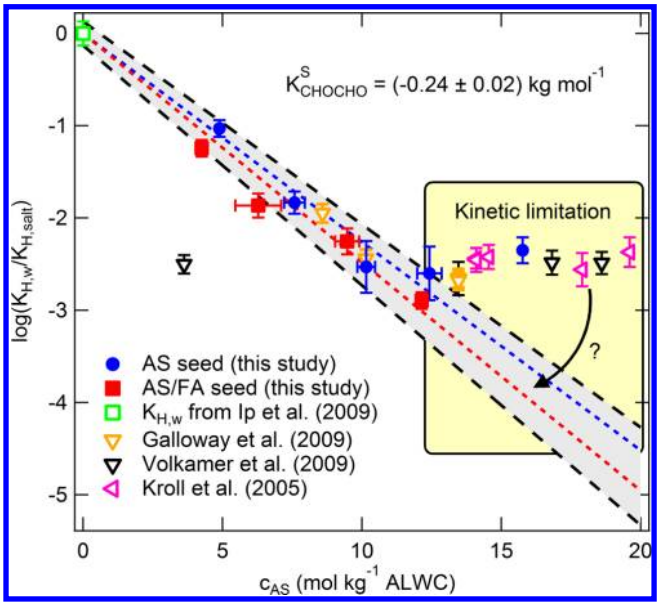

Figure 1. Modified Setschenow plot for glyoxal Henry's law coefficients using 4.19 × 10^5 m atm^{-1} as the Henry's law coefficient of glyoxal in pure water.[31,37] Data shown for this work is based on $K_{H,eff}$ values determined by glyoxal aerosol concentration measurements using filter sampling followed by offline HPLC-ESI-MS/MS.

For Figure 1 $K_{H,w}$ (converted into mol kg^{-1} assuming unit density for pure water from Ip et al.[31]) was divided by the $K_{H,eff}$ values for filter samples, which were lumped into bins of c_{AS} for both seed types used in this study, equaling $K_{H,salt}$ in eq 3. A bivariant linear regression, taking into account both x- and y-errors, gave the following equation:

$$\log\left(\frac{K_{H,w}}{K_{H,salt}}\right) = (0.00 \pm 0.13) + (-0.24 \pm 0.02)m^{-1} \times c_{AS} \quad (3)$$

The intercept represents the measurement uncertainty of $K_{H,eff}$ (or $K_{H,salt}$, respectively) for glyoxal in pure water. From eq 3, K^S_{CHOCHO} was determined to be (−0.24 ± 0.02) m^{-1}. Seed separated analyses indicate that FA does not influence the salting effect significantly. K^S_{CHOCHO} for AS (K^S_{CHOCHO} = −0.25 ± 0.01 m^{-1}) and AS/FA (K^S_{CHOCHO} = −0.23 ± 0.01 m^{-1}) seed are indistinguishable within error bars. Literature $K_{H,eff}$ values were normalized to a density of 1.69 g cm^{-1} for glyoxal SOA[58] and aerosol liquid water as the partitioning volume for glyoxal. Values from Volkamer et al.[35] were additionally corrected for hygroscopicity (κ = 0.24),[32] since wet particle diameters were measured. The c_{AS} values for literature data were calculated using AIM-IV,[51,52] assuming pure AS seed aerosols at the respective RH.

Equation 3 covers a c_{AS} range relevant for SOA as well as fog/cloud droplets, as the liquid water content for SOA (1−100 μg m^{-3}) and fog/cloud droplets (0.1−1 g m^{-3}) differs by 3−6 orders of magnitude,[31] and can provide a means to calculate $K_{H,eff}$ for glyoxal over a wide range of atmospherically relevant particle or droplet sizes. While the salting constant does not seem to depend on the presence of substantial amounts of FA, it should be noted that the salting constants for a given organic compound (here glyoxal) are expected to differ for different inorganic ions. Therefore, the actual $K_{H,eff}$ for glyoxal in atmospheric aerosols depends on the composition of inorganic ions in the aerosols. Gorden and Thorne showed that the total salting constant for seawater is the sum of the products of the molar fractions of the ionic species present and the respective salting constants for those ions.[59,60] K^S_{CHOCHO} for ammonium nitrate and sodium chloride are of special interest, as those salts make up large fractions of aerosols in polluted and marine environments, respectively. However, the small difference between AS and AS/FA seeds simplifies the parameterization of glyoxal partitioning in atmospheric models that often contain mixtures of inorganic and organic (SOA) components. Figure 1 is discussed in context with the literature in Section 3.4.

3.2. Temporal Behavior of Glyoxal Uptake onto Seed Aerosols. Fast uptake of glyoxal was observed in all experiments, followed by a slower increase in the effective Henry's law coefficients over several hours. This increase is partially masked by the strong effect of sulfate molality (see Section 3.1). Figure 2 shows $K_{H,eff}$ values from all filter samples normalized to c_{AS} = 12 m in order to isolate the temporal behavior from c_{AS} effects, and maximize the number of samples for further analysis. This threshold concentration is somewhat arbitrary. Twelve m is chosen because at higher c_{AS} deviation

dx.doi.org/10.1021/es400083d | Environ. Sci. Technol. 2013, 47, 4236−4244

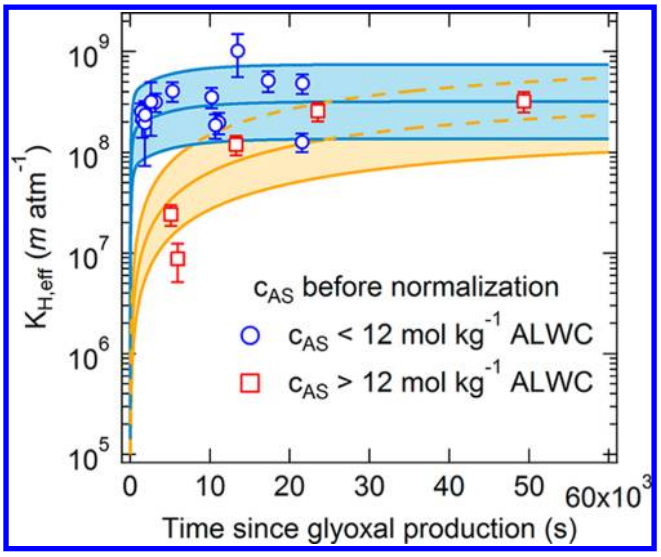

Figure 2. Temporal evolution of glyoxal partitioning expressed as bivariant exponential functions. $K_{H,eff}$ values were normalized to c_{AS} = 12 m. Colored areas reflect the uncertainty in $K_{H,eff}^{eq}$ as derived from eq 3 (see text).

from the expected behavior in the modified Setschenow plot occurred (see Figure 1). Normalization was achieved by applying a correction factor to the measured $K_{H,eff}$ values, which was the ratio of $K_{H,eff}$ at c_{AS} = 12 m and $K_{H,eff}$ at the actual c_{AS} for the respective sample, calculated using eq 3. Time information across one experiment was maintained by applying the correction factor obtained for samples collected at later stages of the experiment also to the previous ones. We propose a bivariant exponential description of two reservoirs of glyoxal in the particle-phase to describe the overall glyoxal uptake behavior:

$$K_{H,eff}(t) = K_{H,eff}^{eq} - A_1 \times e^{-t/\tau_1} - A_2 \times e^{-t/\tau_2} \quad (4)$$

where $K_{H,eff}(t)$ is the observed Henry's law coefficient at a given time (m atm^{-1}), $K_{H,eff}^{eq}$ is the Henry's law coefficient in equilibrium (m atm^{-1}), A_1 and A_2 are the components of $K_{H,eff}^{eq}$ attributed to reservoir 1 and reservoir 2 (m atm^{-1}), and τ_1 and τ_2 are the characteristic time constants for the build-up processes of reservoir 1 and reservoir 2, respectively. The overall reversible glyoxal pool in the particle-phase is given by $A_1 + A_2 = K_{H,eff}^{eq}$, while the increase of K_H due to reservoir 2 in equilibrium is given by $A_2/A_1 = K_{olig}$. Reservoir 1 can be interpreted as the species present after the initial partitioning of glyoxal to the particle-phase, e.g. dehydrated glyoxal monomer, glyoxal monohydrate, and glyoxal dihydrate; while reservoir 2 builds up with a much longer characteristic time constant τ_2 and can therefore be interpreted as the pool of higher molecular weight glyoxal oligomers.

Time constants of $\tau_1 = 2.5 \times 10^2$ s and $\tau_2 = 5.5 \times 10^3$ s are the best-fit values for the $K_{H,eff}$ data at c_{AS} < 12 m before normalization in Figure 2. For the best-fit of the $K_{H,eff}$ data originally c_{AS} > 12 m, longer time constants were required, i.e. $\tau_1 = 4.4 \times 10^4$ s and $\tau_2 = 4.7 \times 10^4$ s. This indicates slower kinetics for the particle-phase reactions of glyoxal, i.e. hydration and oligomerization reactions at high salt concentrations, potentially because fewer water molecules are available for reactions and/or particle viscosity has increased. $K_{H,eff}^{eq}$ for the fits was 3.18×10^8 m atm^{-1} as derived from eq 3 at 12 m c_{AS}. The uncertainties related to eq 3 are reflected in the light colored areas.

Over the course of each experiment K_{olig} was observed to be between 0.5 and 2 (not shown), which corresponds to the enhancement of $K_{H,eff}$ at later stages of the experiments compared to the first $10^3 - 5 \times 10^3$ s, according to:

$$K_{H,eff}^{eq} = A_1 \times (1 + K_{olig}) \quad (5)$$

Based on the observed values of K_{olig}, neither the monomer reservoir nor that of the higher molecular weight oligomers ever exceeded 2/3 of the total particle-phase glyoxal at equilibrium, corresponding to $A_2/K_{H,eff}^{eq} < 2/3$, and $A_1/K_{H,eff}^{eq} < 2/3$. Both reservoirs are therefore significant, with the relative importance depending on c_{AS}. For Figure 2, the ratio of A_2/A_1 (= K_{olig}) was thus chosen to be 1 in the case of c_{AS} < 12 m. For c_{AS} > 12 m in Figure 2 K_{olig} was chosen as 0.5 to achieve the best fit. To our knowledge this is the first quantitative experimental estimation of the glyoxal species distribution in model aerosols.

3.3. Method Comparison. Significant discrepancies were observed in the results of the online and the offline methods to quantify glyoxal particle-phase concentrations. We observed that the particulate glyoxal concentrations at early stages (<2 × 10^3 s) of the experiments are underestimated by the PMF analysis.

Figure 3 illustrates that the differences in the $K_{H,eff}$ values calculated using the reversible glyoxal particle-phase concentrations from the filter-based method and the AMS-based method also correlate with c_{AS}. This dependency in the difference suggests that one or both measurement techniques are systematically biased. Additionally, a seed dependence of this effect was observed, as it is more pronounced for AS/FA aerosols. The seed-separated linear regressions (taking into account both x- and y-errors) of $\Delta K_{H,eff}$, binned for c_{AS} intervals

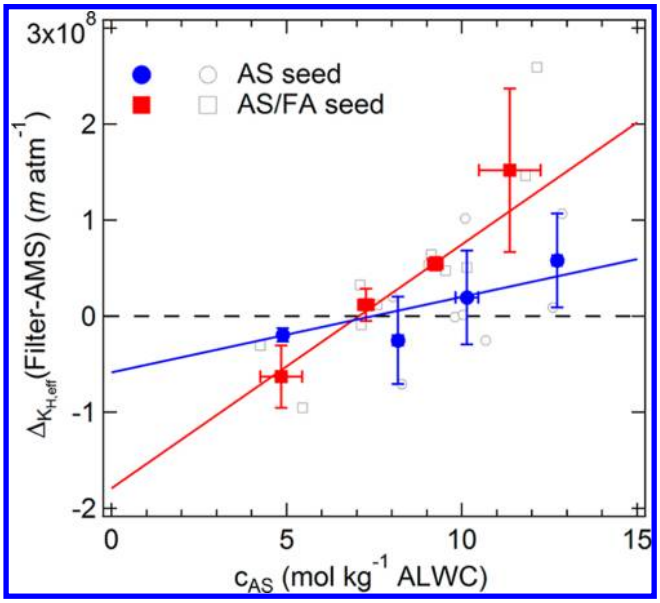

Figure 3. Comparison of particle-phase glyoxal measurement methods. Shown is the difference between $K_{H,eff}$ derived from offline HPLC-MS/MS and AMS measurements as a function of c_{AS}. $K_{H,eff}$ from GLY PMF factor have been averaged for the periods of filter sampling. Error bars reflect standard deviation of the binning process. Closed symbols reflect binned data, while open symbols show nonbinned data.

dx.doi.org/10.1021/es400083d | Environ. Sci. Technol. 2013, 47, 4236−4244

to enhance the visual impression for Figure 3, gave the following fit equations:

$$\text{AS: } \Delta K_{\text{H,eff}} = -0.58 \times 10^8\ m\ \text{atm}^{-1} + 0.79 \times 10^7\ \text{atm}^{-1} \times c_{\text{AS}} \quad (6)$$

$$\text{AS/FA: } \Delta K_{\text{H,eff}} = -1.79 \times 10^8\ m\ \text{atm}^{-1} + 2.54 \times 10^7\ \text{atm}^{-1} \times c_{\text{AS}} \quad (7)$$

As part of the method development process the potential sampling and/or measurement artifacts of the filter sampling offline HPLC-ESI-MS/MS method related to differences in the ionic strength of synthetic samples had been investigated (~ 400 times higher than what could be encountered in the chamber samples).[47,61] For methylglyoxal it was found that the recovery of spikes was reduced by up to 30% in those samples, and hence small effects of salts are possible for glyoxal.[47,61] However, the recovery of glyoxal in the chamber samples is likely reduced by a much smaller percent, since the AS concentrations here were more than 2 orders of magnitude lower. Further, if a bias were present, the observed trend would reflect a lower limit for partitioning at higher c_{AS}, while the opposite trend is observed in Figure 3: the offline method shows higher values at higher c_{AS} compared to the AMS-based method. We therefore attribute this finding to a loss of reversibly partitioned glyoxal species from the aerosols in the aerodynamic lens system of the AMS. This loss is likely due to evaporation of water within the aerodynamic lens inlet of the AMS, leading to removal of gas-phase glyoxal under these reduced pressure conditions. Water loss acts to push and pull a fraction of the easily accessible glyoxal reservoir out of the aerosols, by either (1) lowering the available partitioning volume for glyoxal and thus pushing it out of the aerosols, or (2) shifting the partitioning by removing the gas phase. Despite the short time scale available for evaporation, laboratory measurements suggest the water loss is substantial. For deliquesced AS particles, 80% water loss has been observed within the same type of aerodynamic lens coupled to a different mass spectrometer,[62] while 50−75% water loss from sulfuric acid particles has been observed in the AMS.[54] Notably, Yu et al. showed that in the presence of sulfate ions the distribution among glyoxal monohydrate, glyoxal dihydrate, and glyoxal oligomers is shifted toward the monomer dihydrate, thus resulting in increased hydration and decreased oligomerization.[24] Such effects are likely to prevent oligomerization in increasingly concentrated salt solutions during evaporation.

At the lower end of the ionic strength scale, storage of the filter samples prior to analysis may bias the results. The filter samples were stored at −20 °C, but we cannot rule out that irreversible reactions continue at a slow rate on the filters. Therefore, the difference between the two methods at low ionic strengths might be explained by a negative sampling/storage artifact in the filter method.

3.4. Comparison with Literature. $K_{\text{H,eff}}$ values have been reported in several studies on bulk solutions as well as chamber seed aerosols.[31,33,35,36] While a $K_{\text{H,eff}}$ of $4.2 \times 10^5\ m\ \text{atm}^{-1}$ is reported for pure water,[31] higher values are reported for AS and AS/FA chamber seed aerosols. This is in agreement with a salting-in effect of glyoxal as reported in this study.

We observe $K_{\text{H,eff}}$ values of $1.7 \times 10^8 - 2.3 \times 10^8\ m\ \text{atm}^{-1}$ at later stages (5−10 h after glyoxal production) of dark experiments at 40−80% RH. For comparison with previous chamber studies of dark glyoxal uptake on AS seed we recalculated $K_{\text{H,eff}}$ values for three studies[33,35,36] to compare with this work as described in Section 3.1. The range of values in the absence of OH radicals is $(1.0 \times 10^8$ to $1.5 \times 10^8)\ m\ \text{atm}^{-1}$ at 45−55% RH,[33] and $(1.3 \times 10^8$ to $2.1 \times 10^8)\ m\ \text{atm}^{-1}$ at 56−70% RH,[36] and $(1.0 \times 10^8$ to $1.5 \times 10^8)\ m\ \text{atm}^{-1}$ in the presence of an OH radical source at 46−88% RH.[35] No obvious dependence on OH radicals is visible, consistent with Figure 7B in ref 35. As can be seen in Figure 1 the higher RH values of Galloway et al.[36] fit onto the salting-in behavior observed in this study, while all literature values at moderately low RH (high c_{AS}) were found to deviate from the expected exponential behavior. However, these indications for less pronounced glyoxal uptake at high c_{AS} can be explained by the observed temporal uptake behavior (see Figure 2). The time constants for reservoir 1 and reservoir 2 (τ_1 and τ_2) increased significantly at $c_{\text{AS}} > 12\ m$, indicating the equilibrium for the glyoxal partitioning cannot be reached at the time scales of the respective chamber experiments. The outlier from Volkamer et al.[35] was conducted at RH above the deliquescence RH of AS. Similarly, the authors observed sustained and enhanced uptake for AS/FA seed at RH above the deliquescence RH, and concluded that this observation deserves further attention.[35] Notably, a reanalysis to correct the volume growth[35] for water attracted by glyoxal SOA leads to about a factor of 2 lower K_{Heff} at high RH.[32] This is insufficient to fully explain the outlier point, and suggests that irreversible SOA reactions do contribute additional volume growth at high RH also for AS. This is consistent with previous conclusions about faster SOA formation rates at high RH in AS/FA,[35] which are not the topic of this paper, but supported by our data (see Figure S3).

Although salting-effects have been known since the late 19th century,[37] they are not fully understood mechanistically and are poorly characterized at the very high salt concentrations characteristic of atmospheric aerosols. The general perception is that inorganic ions compete with the dissolved organic compound for water molecules to form hydration-shells. However, for very polar organic compounds, e.g. glyoxal, which can strongly interact with the inorganic ions a salting-in effect may be observed.[38] This physical effect of increased solubility is likely accompanied by a chemical effect in the case of glyoxal, because it is very reactive and its partitioning is largely influenced by chemical reactions in the aqueous-phase, i.e. hydration and oligomerization reactions, subsequent to the actual phase-transition. From a kinetic point of view, the increase in both τ_1 and τ_2 at high c_{AS} can be interpreted as (1) an increased hindrance of the glyoxal uptake, and (2) a slower conversion of monomers into oligomers. This can be explained by (1) an increased particle viscosity, and/or (2) a stabilization of the hydrated monomeric forms by electrostatic interactions with sulfate ions, deactivating them for the oligomerization reactions; or the reversible nucleophilic addition of sulfate ions at the nonhydrated carbonyl carbons deactivates the molecule for further oligomerization. Potentially both mechanisms hindering the oligomerization reactions are active in the particle phase. Additionally, the viscosity of the particles increases with increasing c_{AS}, slowing down all particle-phase reactions. This might also explain differences between bulk studies and chamber studies: e.g. Ip et al.[31] report much higher $K_{\text{H,eff}}$ values at lower salt concentrations ($K_{\text{H,eff}} = 2.4 \times 10^7\ M\ \text{atm}^{-1}$ at a sodium sulfate concentration of 0.01 M) than observed during this study or other chamber studies.[31,33,35,36] However, their values cannot be directly compared to chamber

studies, since the systems investigated differ significantly. Ip et al.[31] investigated glyoxal in sulfate ion containing bulk solutions, while in chamber studies a fully dynamically coupled gas-/particle-phase system is investigated, which is subject to much higher c_{AS} and viscosity effects.

Additionally, we also observed that a shift toward reservoir 1 (monomeric glyoxal species)[24] was necessary to achieve the best-fit for the temporal uptake behavior of samples collected at the highest c_{AS} (see Section 3.2 and Figure 2). Generally we observed the two reservoirs for monomeric and reversibly formed oligomeric species of glyoxal to be of comparable magnitude, which is reflected in the experimentally derived upper limit of $K_{olig} = 2$ (lower limit: $K_{olig} = 0.5$).

3.5. Relevance for Glyoxal SOA Models and Outlook. The enhancement ($\sim 10^3$) observed for reversible glyoxal partitioning between dilute (cloud) conditions (4×10^5 M atm^{-1}, e.g. Ip et al.[31]) and concentrated (aerosol) conditions ($>10^8$ M atm^{-1}, e.g. refs 31−36, and this study), has been described for modeling purposes by means of a simplified equation[32] as:

$$K^*_{H,eff} = K_{H,eff} \times (1 + K_{olig}) \quad (9)$$

with $K_{H,eff}$ as defined in eq 2, $K^*_{H,eff}$ = overall effective Henry's law coefficient in equilibrium, and K_{olig} as the enhancement due to oligomers (compare eq 5). This equation can be interpreted to explain the observed enhancement as either (1) primarily due to the formation of higher molecular weight oligomers, i.e. due to a high K_{olig},[32] or (2) due to an increase in $K_{H,eff}$, i.e. because of the observed salting-in effect, while K_{olig} is ∼1. The results from this work strongly favor the second interpretation. The chemical speciation of the monomer species of glyoxal that are responsible for this enhancement is as yet not well-known, but is relevant for the average O:C ratio of glyoxal SOA, as well as for the availability of unhydrated moieties of glyoxal for irreversible reactions, e.g. imidazole formation,[15,16,20−25] which often require a carbonyl group.

It should be noted that the glyoxal SOA predicted from eq 9 presents a lower limit for total SOA formed from glyoxal, since irreversible reactions are not treated in this manuscript. Notably, while K^S_{CHOCHO} is independent of the presence of FA, the rate of irreversible SOA formation is accelerated by FA.[35] This increased irreversible SOA formation in AS/FA seeds is illustrated in Figure S3, and confirmed in this work. Irreversible SOA will be the topic of an upcoming publication by Waxman et al.

Finally, for the conditions of the April 9, 2003 case study of SOA formation in Mexico City our measurements infer $K_{H,eff} \sim 5 \times 10^7$ m atm^{-1}. This $K_{H,eff}$ value has recently been used to predict SOA formation from glyoxal, including irreversible oxidation reactions, and reactions with NH_4^+. It was found to explain the SOA mass attributed to glyoxal in Mexico City.[63,64]

■ ASSOCIATED CONTENT

Supporting Information

Details on results of offline glyoxal particle-phase analysis and $K_{H,eff}$ calculations, the sensitivity study on MW of Suwannee River Fulvic Acid (SRFA), the modified Setschenow plot using total particle volume for c_{AS} (mol L^{-1}), AMS collection efficiency, PMF analysis of AMS organic mass spectra, and a comparison of AMS and SMPS mass distributions. This information is available free of charge via the Internet at http://pubs.acs.org/.

■ AUTHOR INFORMATION

Corresponding Author

*Phone: +1 (303) 492 1843; e-mail: Rainer.Volkamer@Colorado.edu.

Notes

The authors declare no competing financial interests.

■ ACKNOWLEDGMENTS

We acknowledge the entire team of EUROCHAMP-2 grant E2-2011-03-23-0055, including Barbara Noziere, Rupert Holzinger, and Joseph Timkovsky for their contributions during the campaign and Siyuan Wang for helpful discussions. E.M.W. is recipient of a NSF Graduate fellowship. C.J.K. and T.H. acknowledge the EC project POLYSOA (Polymers in secondary organic aerosols) and the EU-IP EUCAARI (European Integrated project on Aerosol Cloud Climate and Air Quality Interaction) for financial support. U.B. acknowledges financial support from the Swiss National Science Foundation and EUROCHAMP-2. J.G.S. is supported by the SNF through the Ambizione program (grant PZ00P2_131673). R.V. acknowledges financial support from U.S. National Science Foundation CAREER award (ATM-0847793), and U.S. Department of Energy, Office of Science award DE-SC0006080.

■ REFERENCES

(1) Solomon, S.; Qin, D.; Manning, M.; Chen, Z.; Marquis, M.; Averyt, K. B.; Tignor, M.; Miller, H. L; Eds. *Contribution of Working Group I to the Fourth Assessment Report of the Intergovernmental Panel on Climate Change*; Cambridge University Press: Cambridge, UK and New York, 2007.

(2) Kanakidou, M.; Seinfeld, J. H.; Pandis, S. N.; Barnes, I.; Dentener, F. J.; Facchini, M. C.; Van Dingenen, R.; Ervens, B.; Nenes, A.; Nielsen, C. J.; Swietlicki, E.; Putaud, J. P.; Balkanski, Y.; Fuzzi, S.; Horth, J.; Moortgat, G. K.; Winterhalter, R.; Myhre, C. E. L.; Tsigaridis, K.; Vignati, E.; Stephanou, E. G.; Wilson, J. Organic aerosol and global climate modelling: A review. *Atmos. Chem. Phys.* **2005**, *5* (4), 1053−1123, DOI: 10.5194/acp-5-1053-2005.

(3) Zhang, Q.; Jimenez, J. L.; Canagaratna, M. R.; Allan, J. D.; Coe, H.; Ulbrich, I.; Alfarra, M. R.; Takami, A.; Middlebrook, A. M.; Sun, Y. L.; Dzepina, K.; Dunlea, E.; Docherty, K.; DeCarlo, P. F.; Salcedo, D.; Onasch, T.; Jayne, J. T.; Miyoshi, T.; Shimono, A.; Hatakeyama, S.; Takegawa, N.; Kondo, Y.; Schneider, J.; Drewnick, F.; Borrmann, S.; Weimer, S.; Demerjian, K.; Williams, P.; Bower, K.; Bahreini, R.; Cottrell, L.; Griffin, R. J.; Rautiainen, J.; Sun, J. Y.; Zhang, Y. M.; Worsnop, D. R. Ubiquity and dominance of oxygenated species in organic aerosols in anthropogenically-influenced Northern Hemisphere midlatitudes. *Geophys. Res. Lett.* **2007**, *34* (13), L13801 DOI: 10.1029/2007GL029979.

(4) Jimenez, J. L.; Canagaratna, M. R.; Donahue, N. M.; Prevot, A. S. H.; Zhang, Q.; Kroll, J. H.; DeCarlo, P. F.; Allan, J. D.; Coe, H.; Ng, N. L.; Aiken, A. C.; Docherty, K. S.; Ulbrich, I. M.; Grieshop, A. P.; Robinson, A. L.; Duplissy, J.; Smith, J. D.; Wilson, K. R.; Lanz, V. A.; Hueglin, C.; Sun, Y. L.; Tian, J.; Laaksonen, A.; Raatikainen, T.; Rautiainen, J.; Vaattovaara, P.; Ehn, M.; Kulmala, M.; Tomlinson, J. M.; Collins, D. R.; Cubison, M. J.; Dunlea, E. J.; Huffman, J. A.; Onasch, T. B.; Alfarra, M. R.; Williams, P. I.; Bower, K.; Kondo, Y.; Schneider, J.; Drewnick, F.; Borrmann, S.; Weimer, S.; Demerjian, K.; Salcedo, D.; Cottrell, L.; Griffin, R.; Takami, A.; Miyoshi, T.; Hatakeyama, S.; Shimono, A.; Sun, J. Y.; Zhang, Y. M.; Dzepina, K.; Kimmel, J. R.; Sueper, D.; Jayne, J. T.; Herndon, S. C.; Trimborn, A. M.; Williams, L. R.; Wood, E. C.; Middlebrook, A. M.; Kolb, C. E.; Baltensperger, U.; Worsnop, D. R. Evolution of organic aerosols in the atmosphere. *Science* **2009**, *326* (5959), 1525−1529, DOI: 10.1126/science.1180353.

(5) Fu, T.-M.; Jacob, D. J.; Wittrock, F.; Burrows, J. P.; Vrekoussis, M.; Henze, D. K. Global budgets of atmospheric glyoxal and methylglyoxal, and implications for formation of secondary organic aerosols. *J. Geophys. Res. Atmos.* **2008**, *113* (D15), D15303 DOI: 10.1029/2007JD009505.
(6) Stavrakou, T.; Müller, J.-F.; De Smedt, L.; Van Roozendael, M.; Kanakidou, M.; Vrekoussis, M.; Wittrock, F.; Richter, A.; Burrows, J. P. The continental source of glyoxal estimated by the synergistic use of spaceborne measurements and inverse modeling. *Atmos. Chem. Phys.* **2009**, *9* (21), 8431−8446, DOI: 10.5194/acp-9-8431-2009.
(7) Kalberer, M.; Paulsen, D.; Sax, M.; Steinbacher, M.; Dommen, J.; Prevot, A. S. H.; Fisseha, R.; Weingartner, E.; Frankevich, V.; Zenobi, R.; Baltensperger, U. Identification of polymers as major components of atmospheric organic aerosols. *Science* **2004**, *303* (5664), 1659−1662, DOI: 10.1126/science.1092185.
(8) Hastings, W. P.; Koehler, C. A.; Bailey, E. L.; De Haan, D. O. Secondary organic aerosol formation by glyoxal hydration and oligomer formation: Humidity effects and equilibrium shifts during analysis. *Environ. Sci. Technol.* **2005**, *39* (22), 8728−8735, DOI: 10.1021/es0504461.
(9) Liggio, J.; Li, S. M.; McLaren, R. Heterogeneous reactions of glyoxal on particulate matter: Identification of acetals and sulfate esters. *Environ. Sci. Technol.* **2005**, *39* (6), 1532−1541, DOI: 10.1021/es048375y.
(10) Liggio, J.; Li, S. M.; McLaren, R. Reactive uptake of glyoxal by particulate matter. *J. Geophys. Res. Atmos.* **2005**, *110* (D10), D10304 DOI: 10.1029/2004JD005113.
(11) Loeffler, K. W.; Koehler, C. A.; Paul, N. M.; De Haan, D. O. Oligomer formation in evaporating aqueous glyoxal and methyl glyoxal solutions. *Environ. Sci. Technol.* **2006**, *40* (20), 6318−6323, DOI: 10.1021/es060810w.
(12) Zhao, J.; Levitt, N. P.; Zhang, R. Y.; Chen, J. M. Heterogeneous reactions of methylglyoxal in acidic media: Implications for secondary organic aerosol formation. *Environ. Sci. Technol.* **2006**, *40* (24), 7682−7687, DOI: 10.1021/es060610k.
(13) Surratt, J. D.; Kroll, J. H.; Kleindienst, T., E.; Edney, E. O.; Claeys, M.; Sorooshian, A.; Ng, N. L.; Offenberg, J. H.; Lewandowski, M.; Jaoui, M.; Flagan, R.; Seinfeld, J. H. Evidence for organosulfates in secondary organic aerosol. *Environ. Sci. Technol.* **2007**, *41* (2), 517−527, DOI: 10.1021/es062081q.
(14) Surratt, J. D.; Gomez-Gonzalez, Y.; Chan, A. W. H.; Vermeylen, R.; Shahgholi, M.; Kleindienst, T. E.; Edney, E. O.; Offenberg, J. H.; Lewandowski, M.; Jaoui, M.; Maenhaut, W.; Claeys, M.; Flagan, R. C.; Seinfeld, J. H. Organosulfate formation in biogenic secondary organic aerosol. *J. Phys. Chem. A* **2008**, *112* (36), 8345−8378, DOI: 10.1021/jp802310p.
(15) Noziere, B.; Dziedzic, P.; Cordova, A. Products and kinetics of the liquid-phase reaction of glyoxal catalyzed by ammonium ions (NH_4^+). *J. Phys. Chem. A* **2009**, *113* (1), 231−237, DOI: 10.1021/jp8078293.
(16) Shapiro, E. L.; Szprengiel, J.; Sareen, N.; Jen, C. N.; Giordano, M. R.; McNeill, V. F. Light-absorbing secondary organic material formed by glyoxal in aqueous aerosol mimics. *Atmos. Chem. Phys.* **2009**, *9* (7), 2289−2300, DOI: 10.5194/acp-9-2289-2009.
(17) Schwier, A. N.; Sareen, N.; Mitroo, D.; Shapiro, E. L.; McNeill, V. F. Glyoxal-methylglyoxal cross-reactions in secondary organic aerosol formation. *Environ. Sci. Technol.* **2010**, *44* (16), 6174−6182, DOI: DOI 10.1021/es101225q.
(18) Sareen, N.; Schwier, A. N.; Shapiro, E. L.; Mitroo, D.; McNeill, V. F. Secondary organic material formed by methylglyoxal in aqueous aerosol mimics. *Atmos. Chem. Phys.* **2010**, *10* (3), 997−1016, DOI: 10.5194/acp-10-997-2010.
(19) Yasmeen, F.; Sauret, N.; Gal, J.-F.; Maria, P.-C.; Massi, L.; Maenhaut, W.; Claeys, M. Characterization of oligomers from methylglyoxal under dark conditions: A pathway to produce secondary organic aerosol through cloud processing during nighttime. *Atmos. Chem. Phys.* **2010**, *10* (8), 3803−3812, DOI: 10.5194/acp-10-3803-2010.
(20) De Haan, D. O.; Corrigan, A. L.; Smith, K. W.; Stroik, D. R.; Turley, J. J.; Lee, F. E.; Tolbert, M. A.; Jimenez, J. L.; Cordova, K. E.; Ferrell, G. R. Secondary organic aerosol-forming reactions of glyoxal with amino acids. *Environ. Sci. Technol.* **2009**, *43* (8), 2818−2824, DOI: 10.1021/es803534f.
(21) De Haan, D. O.; Tolbert, M. A.; Jimenez, J. L. Atmospheric condensed-phase reactions of glyoxal with methylamine. *Geophys. Res. Lett.* **2009**, *36* (11), L11819 DOI: 10.1029/2009GL037441.
(22) De Haan, D. O.; Hawkins, L. N.; Kononenko, J. A.; Turley, J. J.; Corrigan, A. L.; Tolbert, M. A.; Jimenez, J. L. Formation of nitrogen-containing oligomers by methylglyoxal and amines in simulated evaporating cloud droplets. *Environ. Sci. Technol.* **2011**, *45* (3), 984−991, DOI: 10.1021/es102933x.
(23) Kua, J.; Krizner, H. E.; De Haan, D. O. Thermodynamics and kinetics of imidazole formation from glyoxal, methylamine, and formaldehyde: A computational study. *J. Phys. Chem. A* **2011**, *115* (9), 1667−1675, DOI: 10.1021/jp111527x.
(24) Yu, G.; Bayer, A. R.; Galloway, M. M.; Korshavn, K. J.; Fry, C. G.; Keutsch, F. N. Glyoxal in aqueous ammonium sulfate solutions: Products, kinetics and hydration effects. *Environ. Sci. Technol.* **2011**, *45* (15), 6336−6342, DOI: 10.1021/es200989n.
(25) Kampf, C. J.; Jakob, R.; Hoffmann, T. Identification and characterization of aging products in the glyoxal/ammonium sulfate system - Implications for light-absorbing material in atmospheric aerosols. *Atmos. Chem. Phys.* **2012**, *12* (14), 6323−6333, DOI: 10.5194/acp-12-6323-2012.
(26) Carlton, A. G.; Turpin, B. J.; Altieri, K. E.; Seitzinger, S.; Reff, A.; Lim, H. J.; Ervens, B. Atmospheric oxalic acid and SOA production from glyoxal: Results of aqueous photooxidation experiments. *Atmos. Environ.* **2007**, *41* (35), 7588−7602, DOI: 10.1016/j.atmosenv.2007.05.035.
(27) Altieri, K. E.; Seitzinger, S. P.; Carlton, A. G.; Turpin, B. J.; Klein, G. C.; Marshall, A. G. Oligomers formed through in-cloud methylglyoxal reactions: Chemical composition, properties, and mechanisms investigated by ultra-high resolution FT-ICR mass spectrometry. *Atmos. Environ.* **2008**, *42* (7), 1476−1490, DOI: 10.1016/j.atmosenv.2007.11.015.
(28) Tan, Y.; Perri, M. J.; Seitzinger, S. P.; Turpin, B. J. Effects of precursor concentration and acidic sulfate in aqueous glyoxal-OH radical oxidation and implications for secondary organic aerosol. *Environ. Sci. Technol.* **2009**, *43* (21), 8105−8112, DOI: 10.1021/es901742f.
(29) Tan, Y.; Carlton, A. G.; Seitzinger, S. P.; Turpin, B. J. SOA from methylglyoxal in clouds and wet aerosols: Measurement and prediction of key products. *Atmos. Environ.* **2010**, *44* (39), 5218−5226, DOI: 10.1016/j.atmosenv.2010.08.045.
(30) Lim, Y. B.; Tan, Y.; Perri, M. J.; Seitzinger, S. P.; Turpin, B. J. Aqueous chemistry and its role in secondary organic aerosol (SOA) formation. *Atmos. Chem. Phys.* **2010**, *10* (21), 10521−10539, DOI: 10.5194/acp-10-10521-2010.
(31) Ip, H. S. S.; Huang, X. H. H.; Yu, J. Z. Effective Henry's law constants of glyoxal, glyoxylic acid, and glycolic acid. *Geophys. Res. Lett.* **2009**, *36* (1), L01802 DOI: 10.1029/2008GL036212.
(32) Ervens, B.; Volkamer, R. Glyoxal processing by aerosol multiphase chemistry: Towards a kinetic modeling framework of secondary organic aerosol formation in aqueous particles. *Atmos. Chem. Phys.* **2010**, *10* (17), 8219−8244, DOI: 10.5194/acp-10-8219-2010.
(33) Kroll, J. H.; Ng, N. L.; Murphy, S. N.; Varutbangkul, V.; Flagan, R. C.; Seinfeld, J. H. Chamber studies of secondary organic aerosol growth by reactive uptake of simple carbonyl compounds. *J. Geophys. Res.* **2005**, *110* (D23), D23207 DOI: 10.1029/2005JD006004.
(34) Corrigan, A. L.; Hanley, S. W.; De Haan, D. O. Uptake of glyoxal by organic and inorganic aerosol. *Environ. Sci. Technol.* **2008**, *42* (12), 4428−4433, DOI: 10.1021/es7032394.
(35) Volkamer, R.; Ziemann, P. J.; Molina, M. J. Secondary organic aerosol formation from acetylene (C_2H_2): Seed effect on SOA yields due to organic photochemistry in the aerosol aqueous phase. *Atmos. Chem. Phys.* **2009**, *9* (6), 1907−1928, DOI: 10.5194/acp-9-1907-2009.

(36) Galloway, M. M.; Chhabra, P. S.; Chan, A. W. H.; Surratt, J. D.; Flagan, R. C.; Seinfeld, J. H.; Keutsch, F. N. Glyoxal uptake on ammonium sulphate seed aerosol: Reaction products and reversibility of uptake under dark and irradiated conditions. *Atmos. Chem. Phys.* **2009**, *9* (10), 3331−3345, DOI: 10.5194/acp-9-3331-2009.
(37) Setschenow, J. Über die Konstitution der Salzlösungen auf Grund ihres Verhaltens zu Kohlensäure. *Z. Phys. Chem.* **1889**, *Vierter Band* (1), 117−125.
(38) Almeida, M. B.; Alvarez, A. M.; deMiguel, E. M.; delHoyo, E. S. Setschenow coefficients for naphthols by distribution method. *Can. J. Chem.* **1983**, *61* (2), 244−248, DOI: 10.1139/v83-043.
(39) Paulsen, D.; Dommen, J.; Kalberer, M.; Prévôt, A. S. H.; Richter, R.; Sax, M.; Steinbacher, M.; Weingartner, E.; Baltensperger, U. Secondary organic aerosol formation by irradiation of 1,3,5-Trimethylbenzene-NO_x-H_2O in a new reaction chamber for atmospheric chemistry and physics. *Environ. Sci. Technol.* **2005**, *39* (8), 2668−2678, DOI: 10.1021/es0489137.
(40) Taira, M.; Kanda, Y. Continuous generation system for low-concentration gaseous nitrous acid. *Anal. Chem.* **1990**, *62* (6), 630−633, DOI: 10.1021/ac00205a018.
(41) Hatakeyama, S.; Washida, N.; Akimoto, H. Rate constants and mechanisms for the reaction of OH (OD) radicals with acetylene, propyne, and 2-butyne in air at 297 ± 2 K. *J. Phys. Chem.* **1986**, *90* (1), 173−178, DOI: 10.1021/j100273a039.
(42) Thalman, R.; Volkamer, R. Inherent calibration of a blue LED-CE-DOAS instrument to measure iodine oxide, glyoxal, methyl glyoxal, nitrogen dioxide, water vapour and aerosol extinction in open cavity mode. *Atmos. Meas. Tech.* **2010**, *3* (6), 1797−1814, DOI: 10.5194/amt-3-1797-2010.
(43) Volkamer, R.; Spietz, P.; Burrows, J.; Platt, U. High-resolution absorption cross-section of glyoxal in the UV−vis and IR spectral ranges. *J. Photochem. Photobiol. A: Chem.* **2005**, *172* (1), 35−46, DOI: 10.1016/j.jphotochem.2004.11.011.
(44) Volkamer, R.; Etzkorn, T.; Geyer, A.; Platt, U. Correction of the oxygen interferences with UV spectroscopic (DOAS) measurements of monocyclic aromatic hydrocarbons in the atmosphere. *Atmos. Environ.* **1998**, *32* (21), 3731−3747, DOI: 10.1016/S1352-2310(98)00095-8.
(45) Herman, L. Spectre d'absorption de l'oxygene. *Ann. Phys. (Paris)* **1939**, *11*, 548−611.
(46) Rothman, L. S.; Gordon, I. E.; Barbe, A.; Benner, D. C.; Bernath, P. F.; Birk, M.; Boudon, V.; Brown, L. R.; Campargue, A.; Champion, J.-P.; Chance, K.; Coudert, L. H.; Dana, V.; Devi, V. M.; Fally, S.; Flaud, J.-M.; Gamache, R. R.; Goldman, A.; Jacquemart, D.; Kleiner, I.; Lacome, N.; Lafferty, W. J.; Mandin, J.-Y.; Massie, S. T.; Mikhailenko, S. N.; Miller, C. E.; Moazzen-Ahmadi, N.; Naumenko, O. V.; Nikitin, A. V.; Orphal, J.; Perevalov, V. I.; Perrin, A.; Predoi-Cross, A.; Rinsland, C. P.; Rotger, M.; Simecková, M.; Smith, M. A. H.; Sung, K.; Tashkun, S. A.; Tennyson, J.; Toth, R. A.; Vandaele, A. C.; Vander Auwera, J. The HITRAN 2008 molecular spectroscopic data base. *J. Quant. Spectrosc. Radiat. Trans.* **2009**, *110* (9−10), 533−572, DOI: 10.1016/j.jqsrt.2009.02.013.
(47) Kampf, C. J.; Bonn, B.; Hoffmann, T. Development and validation of a selective HPLC-ESI-MS/MS method for the quantification of glyoxal and methylglyoxal in atmospheric aerosols ($PM_{2.5}$). *Anal. Bioanal. Chem.* **2011**, *401* (10), 3115−3124, DOI: 10.1007/s00216-011-5192-z.
(48) DeCarlo, P. F.; Kimmel, J. R.; Trimborn, A.; Northway, M. J.; Jayne, J. T.; Aiken, A. C.; Gonin, M.; Fuhrer, K.; Horvath, T.; Docherty, K. S.; Worsnop, D. R.; Jimenez, J. L. Field-deployable, high-resolution, time-of-flight aerosol mass spectrometer. *Anal. Chem.* **2006**, *78* (24), 8281−8289, DOI: 10.1021/ac061249n.
(49) Allan, J. D.; Delia, A. E.; Coe, H.; Bower, K. N.; Alfarra, M. R.; Jimenez, J. L.; Middlebrook, A. M.; Drewnick, F.; Onasch, T. B.; Canagaratna, M. R.; Jayne, J. T.; Worsnop, D. R. A generalized method for the extraction of chemically resolved mass spectra from Aerodyne aerosol mass spectrometer data. *J. Aerosol Sci.* **2004**, *35* (7), 909−922, DOI: 10.1016/j.jaerosci.2004.02.007.
(50) Aiken, A. C.; DeCarlo, P. F.; Jimenez, J. L. Elemental analysis of organic species with electron ionization high-resolution mass spectrometery. *Anal. Chem.* **2007**, *79* (21), 8350−8358, DOI: 10.1021/ac071150w.
(51) Friese, E.; Ebel, A. Temperature dependent thermodynamic model of the system H^+−NH_4^+−Na^+−SO_4^{2-}−NO_3^-−Cl^-−H_2O. *J. Phys. Chem. A* **2010**, *114* (43), 11595−11631, DOI: 10.1021/jp101041j.
(52) *Extended AIM Aerosol Thermodynamics Model*; http://www.aim.env.uea.ac.uk/aim/aim.php.
(53) *Humic Substances in the Suwannee River, Goergia: Interactions, Properties, and Proposed Structures*; U.S. Geological Survey, United States Department of the Interior: Denver, CO, 1989; pubs.usgs.gov/of/1987/0557/report.pdf.
(54) Paatero, P.; Tapper, U. Positive matrix factorization: A non-negative factor model with optimal utilization of error estimates of data values. *Environmetrics* **1994**, *5* (2), 111−126, DOI: 10.1002/env.3170050203.
(55) Paatero, P. Least squares formulation of robust non-negative factor analysis. *Chemom. Intell. Lab. Syst.* **1997**, *37* (1), 23−35, DOI: 10.1016/S0169-7439(96)00044-5.
(56) Lanz, V. A.; Alfarra, M. R.; Baltensperger, U.; Buchmann, B.; Hueglin, C.; Prevot, A. S. H. Source apportionment of submicron organic aerosols at an urban site by factor analytical modelling of aerosol mass spectra. *Atmos. Chem. Phys.* **2007**, *7* (6), 1503−1522, DOI: 10.5194/acp-7-1503-2007.
(57) Ulbrich, I. M.; Canagaratna, M. R.; Zhang, Q.; Worsnop, D. R.; Jimenez, J. L. Interpretation of organic components from positive matrix factorization of aerosol mass spectrometric data. *Atmos. Chem. Phys.* **2009**, *9* (9), 2891−2918, DOI: 10.5194/acp-9-2891-2009.
(58) De Haan, D. O. *Personal Communication*, 2010.
(59) Gordon, J. E.; Thorne, R. L. Salt effects on the activity coefficient of naphthalene in mixed aqueous electrolyte solutions. I. Mixtures of two salts. *J. Phys. Chem.* **1967**, *71* (13), 4390−4399, DOI: 10.1021/j100872a035.
(60) Gordon, J. E.; Thorne, R. L. Salt effects on non-electrolyte activity coefficients in mixed aqueous aqueous electrolyte solutions. II. Artificial and natural sea waters. *Geochim. Cosmochim. Acta* **1967**, *31* (12), 2433−2443, DOI: 10.1016/0016-7037(67)90013-0.
(61) Kampf, C. J. Quantification and characterization of reactive α-dicarbonyl compounds in atmospheric aerosols. PhD Dissertation, Johannes Gutenberg-Universität Mainz, Mainz, Germany, 2012.
(62) Zelenyuk, A.; Imre, D.; Cuadra-Rodriguez, L. A. Evaporation of water from particles in the aerodynamic lens inlet: An experimental study. *Anal. Chem.* **2006**, *78* (19), 6942−6947, DOI: 10.1021/ac061184o.
(63) Volkamer, R.; San Martini, F.; Molina, L. T.; Salcedo, D.; Jimenez, J. L.; Molina, M. J. A missing sink for gas-phase glyoxal in Mexico City: Formation of secondary organic aerosol. *Geophys. Res. Lett.* **2007**, *34* (19), L19807 DOI: 10.1029/2007GL030752.
(64) Waxman, E. M.; Dzepina, K.; Ervens, B.; Lee-Taylor, J.; Aumont, B.; Jimenez, J. L.; Madronich, S.; and Volkamer, R.; Secondary organic aerosol formation from semi- and intermediate-volatility organic compounds and glyoxal: Relevance of O/C as a tracer for aqueous multiphase chemistry. *Geophys. Res. Lett.* **2013**, DOI: 10.1002/grl.50203.

NOTE ADDED AFTER ASAP PUBLICATION

Due to a production error, this article published April 15, 2013 with errors throughout the text. The correct version published April 18, 2013.